Journal of Physics: Conference Series **3173** (2026) 012041 doi:10.1088/1742-6596/3173/1/012041

An experimental platform to investigate the propagation of turbulent fluctuations in a lung model

A. Ravaioli[1], **G. Santi**[2], **B. Bortolani**[3], **E. Marcelli**[4,5], **A. Benassi**[6], **A. Talamelli**[1] **and G. Bellani**[1]

[1]Department of Industrial Engineering, University of Bologna, Forlì, Italy
[2]Aerospace - Interdepartmental Center for Industrial Research (CIRI-Aerospace), University of Bologna, Bologna, Italy
[3]eDIMES Lab – Laboratory of Bioengineering, Department of Medical and Surgical Sciences (DIMEC), University of Bologna, Bologna, Italy
[4]Health Sciences and Technologies – Interdepartmental Center for Industrial Research (CIRI-SDV), University of Bologna, Bologna, Italy
[5]IRCCS Azienda Ospedaliero-Universitaria di Bologna, Italy
[6]Chiesi Farmaceutici S.p.A., Parma, Italy

E-mail: alex.ravaioli2@unibo.it

Abstract. Understanding airflow dynamics and aerosol deposition in lung airways is crucial for advancing respiratory therapies. However, the complex hierarchical structure of the lung, characterised by up to 23 generations of asymmetrically branching airways, poses significant challenges for both numerical simulations and experimental investigations, particularly in capturing turbulent fluctuations deep within the respiratory tract. In this study, we introduce an experimental platform designed to investigate the propagation of turbulent fluctuations in a simplified lung model. Our approach employs a 3D-printed, rigid, planar airway geometry that represents generations 5 to 7. Hot-wire anemometry, with three probes strategically placed along the centerlines of the branches, is used to measure the flow regimes and fluctuation characteristics simultaneously at multiple locations, under various inlet conditions. Preliminary results indicate that, for a quasi-laminar inlet flow ($Re \approx 1200$), turbulence is generated after the first bifurcation (G_5), while a fully turbulent inlet flow (due to a 90° sharp inlet bend and $Re \approx 1200$) induces an observable energy decay through subsequent generations (G_6, G_7). These findings provide complementary insights to CFD analyses, underscoring the need for further investigation into the mechanisms of turbulent propagation in the lung.

1 Introduction

The respiratory airways comprise a complex three-dimensional network of branches of varying diameters and lengths. This particular geometry poses several challenges in the study of the corresponding flow field. Understanding the flow features in the lung airways can both enhance the development of more sophisticated devices for drug delivery, like inhalers, but also give important insights into the physics of the flow field in the presence of subsequent bifurcations [1].

In the human lung, airway branches progressively subdivide from the throat to the alveoli, leading to reductions in both flow rate and branch diameter with increasing generation. Since the volumetric flow rate decreases more rapidly than the diameter, the Reynolds number declines accordingly, resulting in a gradual yet pronounced reduction and a reverse transition in flow regime—from turbulent near the throat to mixed, and eventually laminar, conditions in the distal airways [2]. The flow evolution, as well

Journal of Physics: Conference Series **3173** (2026) 012041 doi:10.1088/1742-6596/3173/1/012041

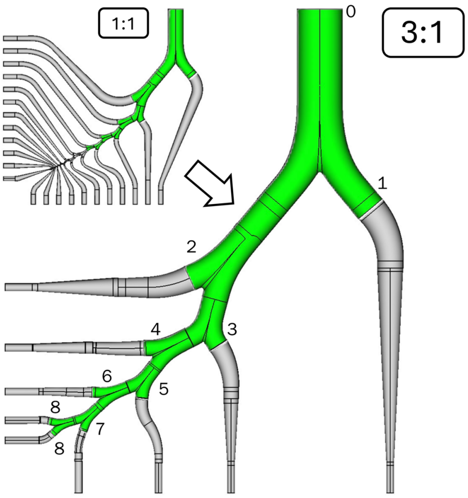

Figure 1: 23 generations model proposed by Möller et al. [4], and 3:1 scaled up model until generation 8 of the present work.

as the generation at which relaminarisation occurs, is strongly influenced by the flow rate at generation 0 (throat). Due to the complex lung geometry, CFD simulations are the only feasible way to study the flow field while maintaining an accurate anatomical structure. However, the literature lacks experimental data to validate the results of the simulations obtained using simplified turbulence models, such as RANS and LES. Therefore, the nature of velocity fluctuations and the spectra in the deeper generations remain to be clarified [3].

For this reason, it was decided to experimentally investigate the flow features and spectra from the throat to deeper generations, as well as the influence of inlet conditions, by employing a new experimental platform with multiple measurement stations suitable for both singular and multiple hot-wire measurements. The overall description of the experimental platform is provided with a focus on the setup of the three deepest generations that the entire platform will comprise, and the results of the investigation of nine inlet conditions on these three subsequent bifurcations. The inlet conditions consist of the combination of three inlet supply ducts and three flow rates. The flow regime is qualitatively analysed by showing energy spectra at each generation.

2 Experimental setup

To enable hot-wire measurements, only an idealised lung model was deemed feasible. For this purpose, the rigid planar model developed by Möller et al. [4] was adopted, originally comprising 23 generations. This model is well suited for hot-wire anemometry and other intrusive measurement techniques, as it features only one accessible branch per generation, while the other branch is vented and used for flow rate regulation. A one-dimensional analysis was carried out to identify the deepest generation suitable for hot-wire measurements. The applicability limit of the technique was set at a bulk velocity of 0.2 m/s and a branch diameter of 10 mm. Moreover, scaling up the models results in lower bulk velocities to preserve dynamic similarity. Based on these considerations, the airways model was limited to generations G_0–G_8, with the last measuring station located at G_7, as shown in Figure 1.

The model is entirely 3D printed with a modular arrangement due to the large final size. The current study involves only the last part of the model, from G_5 to G_8, considered the most critical one in terms of branch diameter and low bulk velocities. Each generation presents a measurement station (1.5 diameters upstream of the bifurcation) in which the hot-wire probe can be inserted inside the branch through 3D-printed seals specifically designed to be adapted to the lung model and probe body. The supply ducts feature two measurement stations, located one diameter downstream from the inlet and one diameter upstream from the outlet. The entire G_0-G_8 experimental platform and the G_5-G_8 part with its measurement stations are shown in Figure 2. The internal walls of the 3D-printed model exhibit an almost smooth surface finish. To study the feasibility of hot-wire measurements and the effect of inlet conditions on the three subsequent bifurcations, three different supply ducts were designed to simulate different conditions upstream of G_5: a short (4D) and a long (10D) straight duct, and a sharp 90° bent

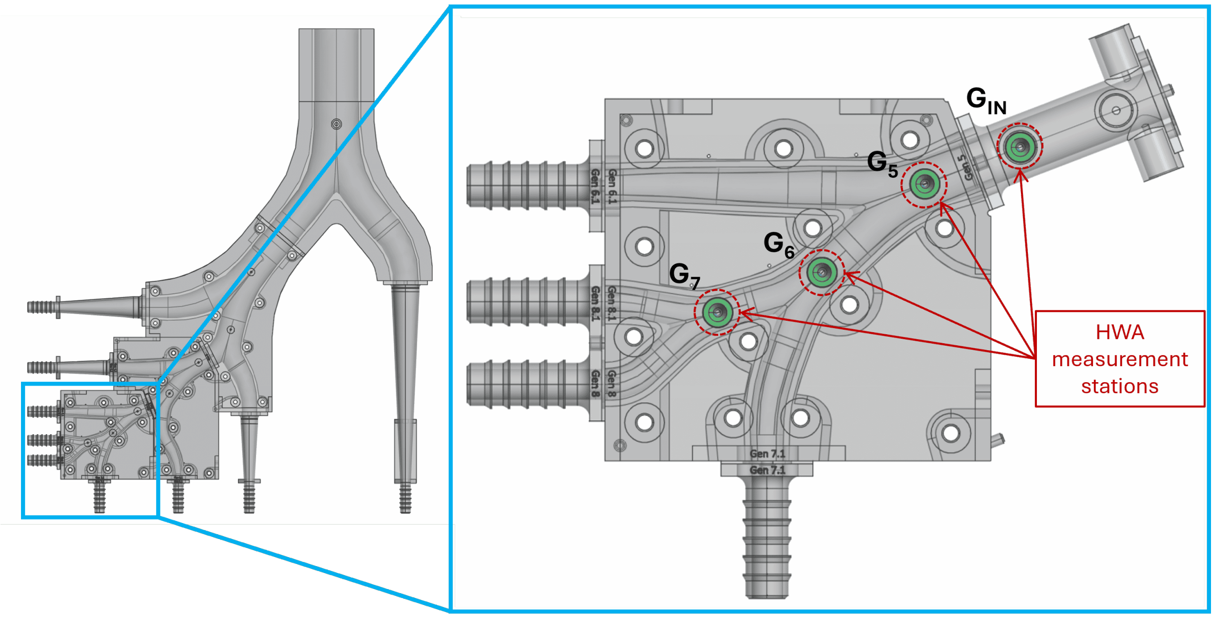

Figure 2: G_0-G_8 model adapted for hot-wire measurements and G_5-G_8 part considered in the present work. The four measurement stations are 1.5 diameters upstream of the bifurcation at each generation.

duct. The schematics are shown in Figure 3. The $G_5 - G_8$ model is supplied by a blower wind tunnel that delivers laminar flow to the supply ducts. The flow rate of each generation is controlled by valves and measured by the pressure losses through orifice plates designed to maximise the range of the highly accurate 26 Pa full-scale pressure transducer. The flow rate ratios of each generation, as well as further details on the airways model, can be found in the work by Möller et al. [4].

2.1 Hot-wire anemometers and low velocity calibration challenges

The hot-wire anemometers were custom-built, with a probe body diameter of 1.6 mm and a single Platinum–Rhodium wire of 2.5 µm in diameter and 0.5 mm in length. Measurements were performed using a DANTEC StreamLine 90N10 system. Owing to the extremely low velocities investigated, a highly accurate calibration procedure was required to minimise measurement uncertainties. For this purpose, the vortex-shedding calibration technique was compared against a commercial calibration unit.

The vortex-shedding technique consists of placing the hot-wire probe at a specific location downstream of a cylinder of known diameter. By measuring both the mean flow velocity and the vortex-shedding

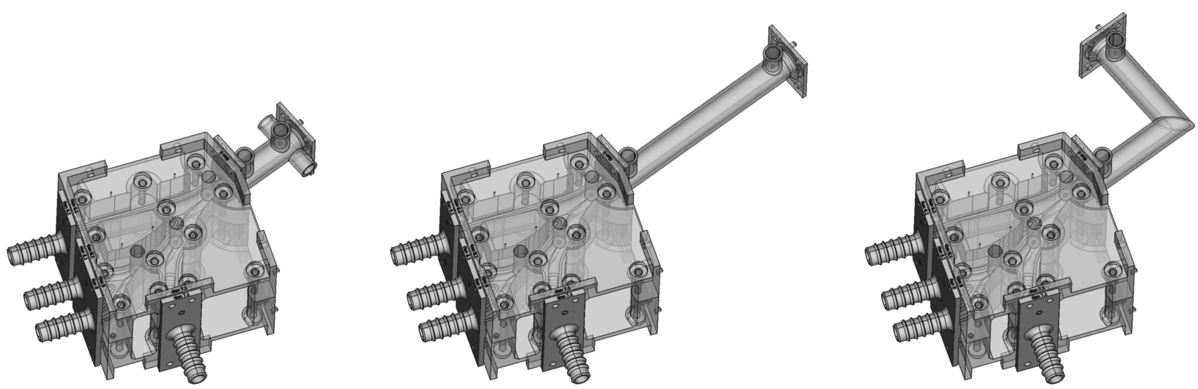

Figure 3: Schematics of the $G_5 - G_8$ lung model with the three different supply ducts tested. From left to right, the short (4D) straight duct, the long (10D) straight duct and the sharp 90° bent duct.

frequency of the cylinder through the hot-wire anemometer, a calibration curve can be obtained without relying on a pressure transducer (which generally exhibits low accuracy below 1 m/s). Figure 4 shows the calibration setup for the vortex-shedding technique. The cylinder is mounted transversely in a pipe of 1.67 cm diameter, which features a measuring station downstream of the cylinder. The duct is connected to the same blower wind tunnel previously described.

Typically, the vortex-shedding calibration technique is applied near the centreline of a large-section wind tunnel, where the velocity profile can be considered uniform. Here, however, the pipe diameter is small compared to that of the cylinder and the hot-wire, making it necessary to account for velocity profile effects. For this reason, both the hot-wire and the cylinder were placed symmetrically with respect to the pipe centreline. Two cylinders of different diameters (1.27 mm and 2.11 mm) were employed to cover a suitable velocity range, since in the transitional regime ($150 < Re < 300$) there is no univocal relationship between Strouhal and Reynolds numbers [5]. Following the work by Sattarzadeh et al. [6], the vertical and axial offsets of the wire relative to the cylinders were $3.9D$ and $5.5D$ for $D = 1.27$ mm, and $2.4D$ and $3.3D$ for $D = 2.11$ mm, respectively. Due to the small diameter size of the duct, the cylinders have a blockage on the flow of approximately 7% and 12%, respectively for $D = 1.27$ mm and $D = 2.11$ mm.

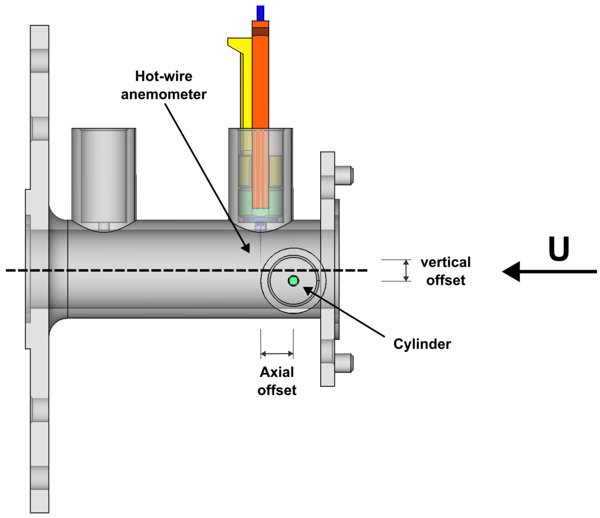

Figure 4: Schematic of the setup exploited for the vortex-shedding calibration. The cylinder and the hot-wire anemometers present a vertical and an axial offset to maximise the energy content at the fundamental frequency while maintaining an accurate measurement of the mean velocity. The vertical and axial offsets of the wire relative to the cylinders are $3.9D$ and $5.5D$ for $D = 1.27$ mm, and $2.4D$ and $3.3D$ for $D = 2.11$ mm, respectively. The cylinder and the hot-wire are placed symmetrically at 2.5 mm with respect to the centreline.

The calibration curve obtained from the vortex-shedding technique was compared with that provided by the DANTEC calibration unit, which enables accurate calibrations at velocities below 1 m/s. The calibration followed the modified King's law, which accounts for natural convection effects [7]. Since the DANTEC calibrator operates with compressed air, its thermophysical properties differ from those of ambient air. Therefore, temperature effects were explicitly considered, as even small differences may induce significant relative errors at low velocities, where $dE/dU \ll 1$. Humidity also affects convective heat transfer, but it was neglected here, given its comparatively minor influence relative to temperature [8]. Literature reports significant humidity effects only at extremely low velocities below 0.1 m/s [9].

Figure 5a shows the calibration curves obtained with the vortex-shedding technique and the commercial calibration unit. A relevant difference in the measured voltage can be noticed in the velocity range between 0 and 3 m/s. Furthermore, below 0.8 m/s (corresponding to $Re_D \approx 100$), it was no longer possible to detect the vortex-shedding frequency. The two calibration curves show good agreement above 3 m/s.

Owing to the more complex procedure, the impossibility of calibrating the hot-wire anemometer below 0.8 m/s, and the additional uncertainties due to wall interaction and velocity profile effects that

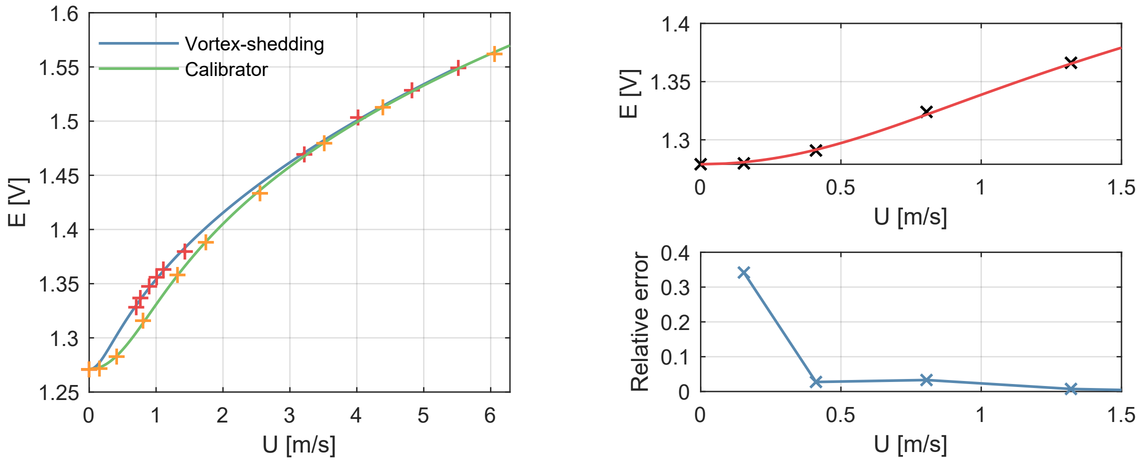

(a) (b)

Figure 5: (a): Comparison of calibration curves obtained with the vortex-shedding technique and the DANTEC calibration unit. Red and orange crosses indicate the calibration points of the vortex-shedding and calibrator methods, respectively. (b): close-up of the calibration curve at low velocity obtained with the DANTEC calibrator and its regression error. Crosses indicate the calibration points.

are extremely challenging to quantify, the commercial calibration unit was preferred over the vortex-shedding technique, despite the temperature corrections required with the DANTEC system.

Figure 5b shows a close-up of the calibration curve obtained with the DANTEC calibrator at low velocities, as well as the regression error. It can be observed that above 0.4 m/s the fitting error remains below 5%.

Hand-crafted anemometers with very fine wires, such as those used in the present study, are prone to drift. To compensate for this, the hot-wire voltage at rest was periodically measured throughout the experiment, enabling adjustments to the calibration curve based on the current E_0.

2.2 Experimental framework

The experimental campaign was designed to investigate the influence of inlet conditions and flow rate on fluctuations and flow regime in the three subsequent bifurcations from generation 5 to 7. The inlet conditions were not intended to reproduce the realistic flow field that would develop at generation 5 from upstream airways, but rather to study the bifurcation system itself within a realistic range of Reynolds numbers compatible with the deep lung region. Along with the investigation of the flow features, the campaign also served as a feasibility study to assess the operability of the experimental platform and the accuracy and usage of custom-built hot-wire anemometers in small-diameter ducts at very low velocities.

A total of nine configurations were tested, combining three inlet Reynolds numbers ($Re \approx 300$, $Re \approx 600$, $Re \approx 1200$) with the three distinct inlet geometries previously described and shown in Figure 3. The Reynolds number tested corresponds to a typical large range of breathing flow rates, namely 30 L/min, 60 L/min and 120 L/min. Data were acquired simultaneously by four hot-wire anemometers at 20 kHz in the positions highlighted in Figure 2: G_{IN}, G_5, G_6 and G_7. Table 1 shows the Reynolds number at each measurement station for the three flow rates tested. The flow rates indicated correspond to the actual volumetric flow through the model's throat (G_0). Note that, for similarity with physiological Reynolds numbers, the effective flow rate in the scaled model is three times higher.

3 Results

The qualitative analysis of the flow regime begins with the characterisation of the three supply ducts, followed by the energy spectra at each generation. The nomenclature of the measurement stations refers to Figure 2. Table 2 shows the turbulence intensity (defined as $Tu = u'/U$, where u' is the root-mean-square of the turbulent velocity fluctuations and U is the mean velocity) measured at G_{IN} for all cases. It can be observed that the turbulence intensity is below 1% for both straight ducts. In addition, the energy spectra of the two straight ducts exhibit an overlapping trend, suggesting that even at $Re \approx 1200$, the flow remains laminar regardless of the duct length. In contrast, the sharp 90° bend triggers transition to

Journal of Physics: Conference Series **3173** (2026) 012041 doi:10.1088/1742-6596/3173/1/012041

	$Q = 30\,\mathrm{L/min}$	$Q = 60\,\mathrm{L/min}$	$Q = 120\,\mathrm{L/min}$
G_{IN}	294	588	1177
G_5	294	588	724
G_6	181	362	451
G_7	113	225	260

Table 1: Reynolds numbers at the measurement stations. The three nominal throat flow rates are 30, 60 and $120\,\mathrm{L/min}$ (G_0), while inlet flow rates are three times higher to preserve Reynolds similarity. Measurements were performed downstream (G_5–G_8), where local flow rates are lower.

a turbulent regime already at $Re \approx 600$. For this reason, only the results for the long straight (10D) and the 90° bent supply ducts are presented in the following, as both straight ducts behave almost identically.

	$Re \approx 300$	$Re \approx 600$	$Re \approx 1200$
Straight duct (4D)	0.4%	0.6%	0.5%
Straight duct (10D)	0.4%	0.4%	0.4%
90° bend (10D)	0.5%	7.4%	13.0%

Table 2: Turbulence intensity measured at G_{IN} (supply duct) for all the cases.

Figure 6 shows the energy spectra for the straight duct (10D) at $Re \approx 300$ and $Re \approx 1200$. At $Re \approx 300$, the spectra show the same decay at all generations, suggesting that the regime is completely laminar. The energy spectra at $Re \approx 600$ are not shown because the behaviour is very similar to $Re \approx 300$. For $Re \approx 1200$, the spectra indicate a laminar flow at G_{IN} and at G_5, while the anemometers at G_6 and G_7 show a significant increase in energy, suggesting a flow transition. The energy is amplified across all frequencies, and the peaks correspond to those already present at G_{IN}, indicating that the bifurcations introduce no specific energy modes. However, a preliminary analysis revealed that the probe body has an impact on triggering transition mainly at $Re \approx 1200$ as explained in the following section.

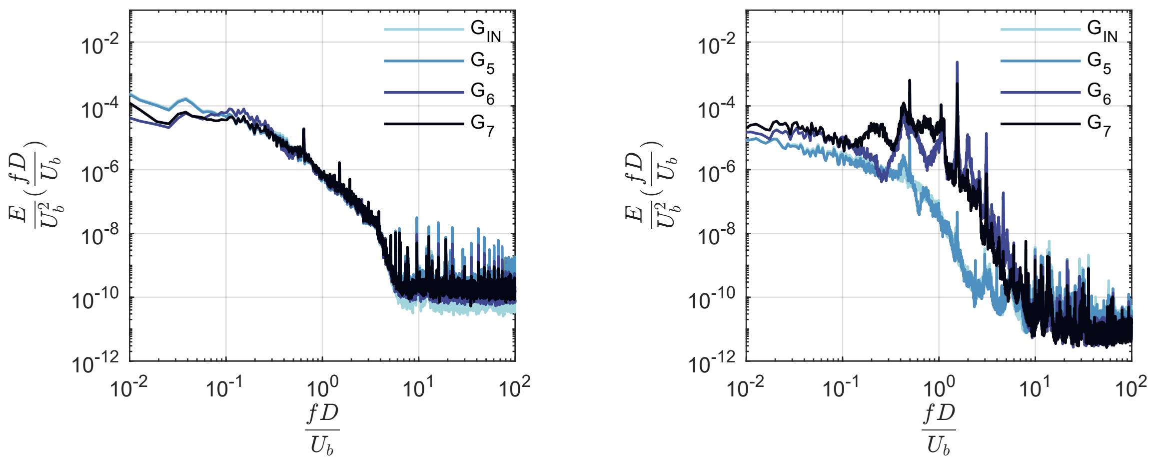

(a) Straight duct (10D), $Re \approx 300$. (b) Straight duct (10D), $Re \approx 1200$.

Figure 6: Energy spectra normalised by the squared bulk velocity at the inlet (G_{IN}) for the straight supply duct (10D) for $Re \approx 300$ and $Re \approx 1200$.

Figure 7 shows the energy spectra at all measurement stations for the 90° bent supply duct for $Re \approx 600$ and $Re \approx 1200$. Spectra at $Re \approx 300$ have not been shown because the trend is very similar to the same flow rate with the straight supply duct, since the flow is completely laminar and no relevant energetic structures are observed. In contrast, at $Re \approx 600$, the spectra assume a turbulence-like behaviour, suggesting that the 90° sharp bend triggers transition to turbulence at very low Reynolds numbers (approximately 600). At this flow rate, a dominant oscillatory motion at $St = 0.12$ is observed, whose energy is about two orders of magnitude greater than the surrounding spectral content. This periodic motion is also observed at deeper generations, although attenuated, and its frequency is consistent with other investigations on 90° bends [10].

At $Re \approx 1200$, the periodic motion is completely absent, contrasting with other studies reporting its presence at higher Reynolds numbers ($Re > 10^4$) [10]. Similarly to the case at $Re \approx 600$, turbulence energy decreases in deeper generations, indicating energy attenuation and a possible relaminarisation if even deeper branches were considered. According to a one-dimensional analysis, the Reynolds number decreases by approximately 40% per generation as shown in Table 1.

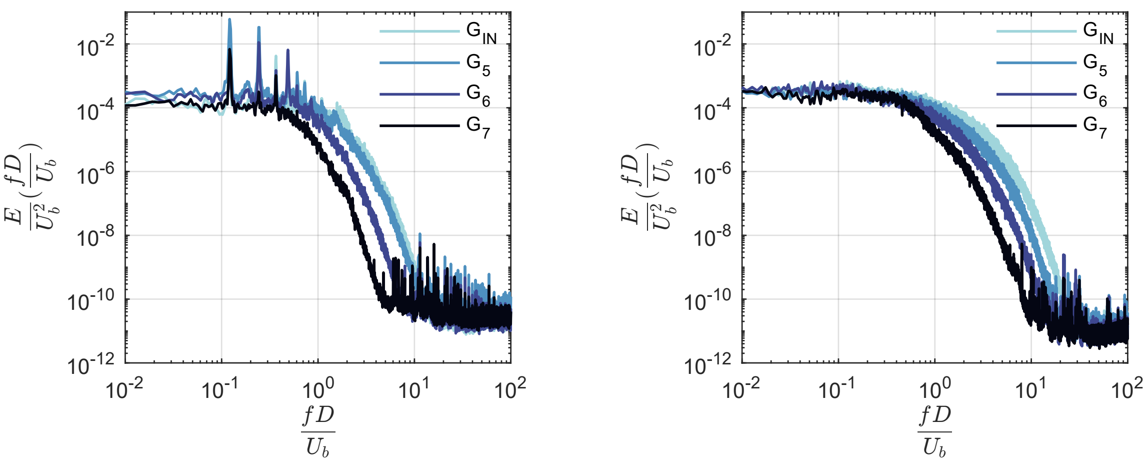

(a) 90° bend, $Re \approx 600$. (b) 90° bend, $Re \approx 1200$.

Figure 7: Energy spectra normalised by the squared bulk velocity at the inlet (G_{IN}) for the 90° bent supply duct and for $Re \approx 600$ and $Re \approx 1200$.

3.1 Sensitivity to a local perturbation

To analyse the effect of a local perturbation on the flow field, a single measuring hot-wire was placed at G_7. Perturbations were then introduced at different locations: only at G_5, only at G_6, and finally at the combination $G_5 + G_6$. As perturbation, a non-measuring hot-wire probe was positioned on the centreline to assess the interference of an upstream hot-wire anemometer on a downstream one. Three flow rates were tested ($Re \approx 300$, $Re \approx 600$, and $Re \approx 1200$) with the straight supply duct.

The energy spectra are shown in Figure 8, exhibiting a strong dependency on Reynolds number, as expected. For $Re \approx 300$ and $Re \approx 600$, no relevant differences are observed. At $Re \approx 1200$, however, a substantial increase in energy appears when the perturbation is applied at G_5, in contrast to the case of perturbation at G_6. This transition at G_5 can be explained by the higher Reynolds number at that location, unlike at G_6.

A more detailed investigation is required to elucidate the underlying physics of this instability.

4 Conclusions

A new experimental platform to study the propagation of fluctuations through successive bifurcations resembling the anatomy of the lung airways was presented. The complete G_0–G_8 model and the experimental setup enabling hot-wire measurements were described, with particular emphasis on the challenges related to low-velocity calibration of the hot-wire probes. Indeed, low velocities are intrinsic in the study of deep airways in a scaled-up model. Preliminary results on the G_5–G_8 region were presented, combining inlet conditions generated by three different supply ducts (two straight ducts of different lengths and a 90° sharp bent duct) and three Reynolds numbers ($Re = 300, 600$, and 1200), in order to investigate the influence of velocity profile and inlet turbulence intensity on the three subsequent bifurcations. In addition, a sensitivity analysis was carried out to evaluate the response to upstream perturbations. The following conclusions can be drawn:

Journal of Physics: Conference Series **3173** (2026) 012041 doi:10.1088/1742-6596/3173/1/012041

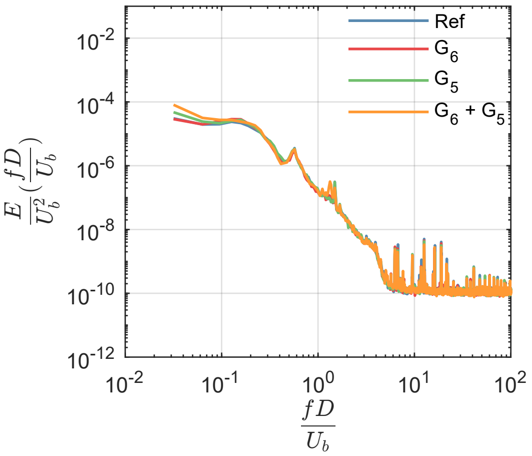

(a) $Re \approx 300$.

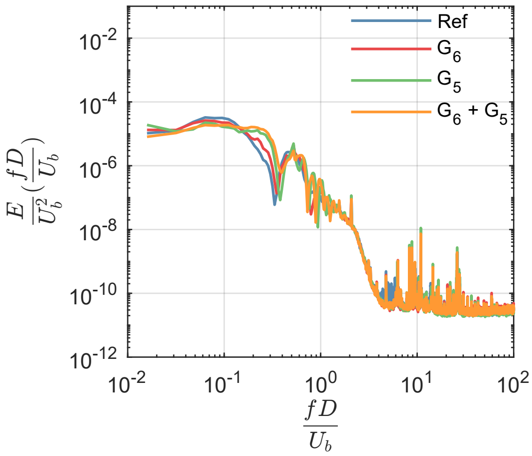

(b) $Re \approx 600$.

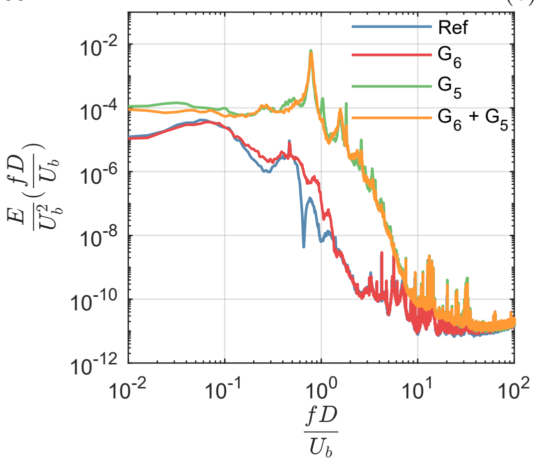

(c) $Re \approx 1200$.

Figure 8: Energy spectra normalised by the squared bulk velocity at the inlet (G_{IN}) measured at G_7, showing the effect of a local perturbation in the positions highlighted in the legend for the straight supply duct and for $Re \approx 300$, $Re \approx 600$ and $Re \approx 1200$. *Ref* is the reference spectrum without any disturbance upstream.

- The short (4D) and long (10D) straight supply ducts show the same behaviour, probably because the Reynolds number is too low to trigger a transition in this tract.
- For the straight supply duct, the laminar regime persists at $Re \approx 300$ and $Re \approx 600$ in all the generations.
- For the straight supply duct at $Re \approx 1200$ a transition is shown at G_6. After a preliminary investigation, it was found that the anemometer's body has a significant impact in triggering the transition to turbulence downstream, leading to the necessity of performing measurements with a single hot-wire at a time to avoid interference effects. Since the measurements in the present study were taken simultaneously at the four stations, the results at $Re \approx 1200$ may have been influenced by flow interactions between stations.
- The 90° sharp bent duct shows an anticipated transition already at $Re \approx 600$, and periodic motion characteristic of 90° bends is observed to be propagated through generations. Turbulence decay is observed from G_5 to G_7.
- For the 90° sharp bent duct at $Re \approx 1200$, no more periodic motion is noticed, and turbulent-like spectra with turbulence energy decay through generations are observed.

This analysis presents inevitable limitations with respect to the flow field in real airways, mainly due to significant geometrical differences such as the model's planarity, rigidity, and surface finish. Nevertheless, it provides valuable insight into the flow features within a successive bifurcation system, which can help elucidate the mechanisms behind flow transition and instability in the deep lung regions.

Future work will include an investigation of the entire eight-generation model with an idealised throat geometry, together with a more in-depth analysis of the transition phenomenon using intermittency techniques for its quantitative characterisation, as well as a stability analysis.

References

[1] C. Kleinstreuer and Z. Zhang. Airflow and Particle Transport in the Human Respiratory System. *Annual Review of Fluid Mechanics*, 42(1):301–334, January 2010.

[2] Warren H Finlay. *The mechanics of inhaled pharmaceutical aerosols: an introduction*. Academic press, 2001.

[3] G.H. Spasov, R. Rossi, A. Vanossi, C. Cottini, and A. Benassi. A critical analysis of the CFD-DEM simulation of pharmaceutical aerosols deposition in upper intra-thoracic airways: Considerations on air flow. *Computers in Biology and Medicine*, 170:107948, March 2024.

[4] Georg Möller, Malte Bieber, Stefanie Gürzing, Anja Lena Thiebes, Sarah Klein, Christian Gabriel Cornelissen, and Manuel Armin Reddemann. Transparent 23-generation airway model for experimental investigation of aerosol flow and deposition within the human respiratory tract. *Journal of Aerosol Science*, 156:105782, August 2021.

[5] Anatol Roshko. On the Development of Turbulent Wakes from Vortex Streets, January 1954.

[6] Sohrab S. Sattarzadeh, Athanasia Kalpakli, and Ramis Örlü. Hot-Wire Calibration at Low Velocities: Revisiting the Vortex Shedding Method. *Advances in Mechanical Engineering*, 5:241726, January 2013.

[7] Arne V Johansson and P Henrik Alfredsson. On the structure of turbulent channel flow. *Journal of Fluid Mechanics*, 122:295–314, 1982.

[8] Z. Popiolek, F.E. Jørgensen, A.K. Melikov, M.C.G. Silva, and W. Kierat. Assessment of Uncertainty in Measurements with Low Velocity Thermal Anemometers. *International Journal of Ventilation*, 6(2):113–128, September 2007.

[9] Tingbo Zhou, Zhengke Zhang, Yongqiang Tian, Zhongxiang Xi, Xiaomu Dou, Weidong Liu, Guobiao Zhang, and Chao Gao. A Calibration Facility for Hot-Wire Anemometers in Extremely Low Speed with Air Temperature and Humidity Variable and Controllable. *Applied Sciences*, 14(4):1587, January 2024.

[10] Athanasia Kalpakli Vester, Ramis Örlü, and P. Henrik Alfredsson. Turbulent Flows in Curved Pipes: Recent Advances in Experiments and Simulations. *Applied Mechanics Reviews*, 68(050802), September 2016.